Isotropic Negative Thermal Expansion in beta-Si(NCN)(2) and Its Origin

ARTICLE *in* THE JOURNAL OF PHYSICAL CHEMISTRY C · DECEMBER 2011

Impact Factor: 4.77 · DOI: 10.1021/jp2106583

6 AUTHORS, INCLUDING:

Peter Kroll
University of Texas at Arlington
123 PUBLICATIONS **2,170** CITATIONS
SEE PROFILE

Miria Andrade
Johnson Matthey
4 PUBLICATIONS **52** CITATIONS
SEE PROFILE

Emanuel Ionescu
Technical University Darmstadt
105 PUBLICATIONS **646** CITATIONS
SEE PROFILE

Gerhard Miehe
Technical University Darmstadt
131 PUBLICATIONS **2,405** CITATIONS
SEE PROFILE

THE JOURNAL OF PHYSICAL CHEMISTRY C

ARTICLE

pubs.acs.org/JPCC

Isotropic Negative Thermal Expansion in β-Si(NCN)$_2$ and Its Origin

Peter Kroll,*[,†] Miria Andrade,[‡] Xuehua Yan,[‡,§] Emanuel Ionescu,[‡] Gerhard Miehe,[‡] and Ralf Riedel[‡]

[†]Department of Chemistry and Biochemistry, The University of Texas at Arlington, Arlington, Texas 76001-0065, United States

[‡]Institut für Materialwissenschaft, Technische Universität Darmstadt, Petersenstr. 23, D-64287 Darmstadt, Germany

[§]School of Materials Science & Engineering, Jiangsu University, Zhenjiang 212013, P.R. China

Supporting Information

ABSTRACT:

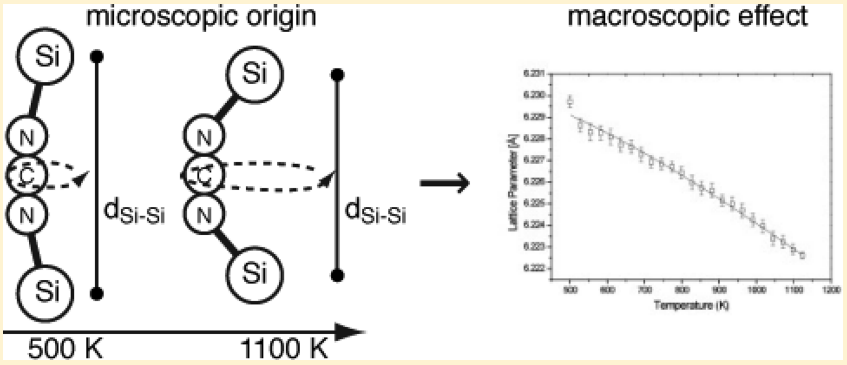

Ab initio molecular dynamic simulations and high-temperature synchrotron crystallography show that β-Si(NCN)$_2$ exhibits isotropic negative thermal expansion from 500 to 1123 K over its entire temperature stability range. The experimental value of the linear expansion coefficient changes from $\alpha = -1.24 \times 10^{-6}$ K^{-1} at 500 K to $\alpha = -1.93 \times 10^{-6}$ K^{-1} at 1123 K. Examination of vibrational motions locate the effect to transverse vibrations of carbodiimide fragments bridging between Si atoms (Si−N═C═N−Si). A detailed atomistic analysis reveals that the roto-vibrational movements of the bridging NCN units resemble that of a centrifugal governor pulling together the crystal framework upon temperature increase.

INTRODUCTION

Contraction upon heating at ambient or elevated temperatures is an exotic phenomenon exhibited by few materials. The best-known example for such negative thermal expansion (NTE) is water, which has its maximum density above its melting point at approximately 4 °C. The majority of materials, however, expand when heated. Upon temperature increase, the anharmonicity of the bonding potential causes an increase in the average bond length, resulting in an expansion of the material.[1−3] Physical origins of NTE, on the other hand, are much more diverse and can be magnetic, electronic, or structural in nature. Fundamental processes include magnetostrictive and displacive phase transitions, valence transition, low-energy phonon modes, and rigid unit modes (RUMs)—all of which can lead to negative contributions to the thermal expansion coefficient.[4−7] And indeed, at cryogenic conditions, many materials show NTE of some kind, but only within a small temperature range.[8,9] At ambient and elevated temperatures, however, negative thermal expansion is still a rare phenomenon, especially when it appears isotropically and over a wide range of temperatures.

Among the few maverick compounds that exhibit isotropic volume contraction at elevated temperatures over a wide range, the family of zirconium tungstate materials are best known and most widely studied. The linear thermal expansion coefficient $\alpha = 1/L(dL/dT)$ of Zr(WO$_4$)$_2$ is about -9×10^{-6} K^{-1} for the range from 0.3 to 1050 K.[9,10] Some cyanide-based framework compounds display an even larger isotropic NTE effect. The NTE coefficients of Zn(CN)$_2$ and isostructural Cd(CN)$_2$ are -16.9×10^{-6} K^{-1} (from 25 to 375 K) and -20.4×10^{-6} K^{-1} (150 to 375 K), respectively.[11,12] These compounds share the structural feature of a network of corner-linked polyhedra connected through metal−oxygen−metal (M−O−M) or metal−cyanide−metal (M−CN−M) bridges. NTE in these materials is commonly explained within the concept of rigid unit modes (RUMs). Low-energy transverse modes of the coordination polyhedra reduce the atomic distance between the anchoring atoms as the temperature is increased.[3,10,13] For example, enhanced geometric flexibility associated with metal−cyanide−metal linkages, as compared to the same structures linked by single atoms, leads to pronounced NTE behavior in cyanide-based framework compounds.[11,12]

Received: November 7, 2011
Revised: December 1, 2011

dx.doi.org/10.1021/jp2106583 | J. Phys. Chem. C XXXX, XXX, 000–000

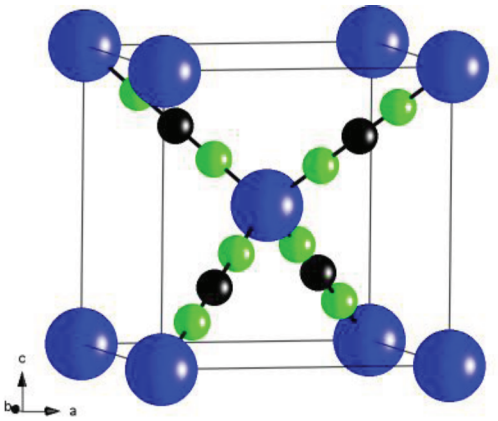

Figure 1. Unit cell of β-Si(NCN)$_2$; space group $Pm\bar{3}m$ (224).

Thermal expansion is a critical parameter that must be considered in the design of materials structures subjected to temperature variations. Therefore, NTE materials potentially can be used for the production of composites with precisely tunable thermal expansion characteristics. Such materials are practical in optical, electronic, biomedical, and engineering applications.[14−16] Consequently, in recent years NTE materials have attracted significant scientific and technological interest. Besides, achieving a detailed understanding on the NTE mechanisms would facilitate the extension of the relatively small category of materials that show isotropic NTE.

In 1997, the ternary crystalline compound SiC_2N_4 was synthesized for the first time.[17] The silicon carbonitride compound is comprised of the carbodiimide $[N{=}C{=}N]^{2-}$ unit as complex anion and has to be described as silicon dicarbodiimide, SiC_2N_4 = Si(NCN)$_2$. Silicon dicarbodiimide exhibits two polymorphs, α and β, which are related by a reversible phase transformation at about 150 °C. The crystal structure of the room-temperature phase, α-Si(NCN)$_2$, has not yet been determined. The high-temperature phase, β-Si(NCN)$_2$, has been structurally characterized by in situ X-ray diffraction; it shows a cubic structure (space group $Pm\bar{3}m$), defined by the lattice constant (a = 6.19 Å) and the nitrogen positional parameter (x = 0.147). It displays the topology of an anticuprite structure, which can be considered as two interpenetrating networks of the high-cristobalite (SiO_2) structure type, with carbodiimide groups replacing the oxygen atoms.[18,19] A unit cell of β-Si(NCN)$_2$ is shown in Figure 1. The apparent linear Si−NCN−Si linkage is a consequence of spatial averaging, as indicated by large static and dynamic anisotropic displacement parameters.[17] Subsequent DFT optimization of β-Si(NCN)$_2$ indeed found a bond angle of 147° at the N atom.[18]

The possibility of NTE in Si(NCN)$_2$, has been reflected about early on.[18] Preliminary theoretical studies using ab initio molecular dynamic simulations indicated a strong NTE effect.[20] In the present work, the thermal expansion behavior of β-Si(NCN)$_2$ has been investigated by in situ synchrotron X-ray powder diffraction and further computational studies were performed to support the findings and to elucidate the phenomenon. Anticipating our results, we show that Si(NCN)$_2$ exhibits strong isotropic negative thermal expansion over a wide temperature range. Furthermore, we propose a mechanism for the NTE behavior of β-Si(NCN)$_2$ based on atomistic simulations.

MATERIALS AND METHODS

Experimental Section. The synthesis of X-ray amorphous Si(NCN)$_2$ was performed as reported elsewhere.[17] The material was calcinated under vacuum at 623 K for 90 min, with subsequent annealing at 973 K for 45 min under argon atmosphere. The C, N, and O content of the ceramics were analyzed by hot gas extraction using a C-Analyzer Leco C-200 and NO-Analyzer Leco TC-436, respectively. The silicon content was estimated by the difference of the sum of the measured carbon, nitrogen, and oxygen content to 100%. The final composition was determined to be $SiC_{1.74}N_{3.45}O_{0.08}$.

In situ synchrotron X-ray powder diffraction experiments were performed on the Beamline ID31 at the European Synchrotron Radiation Facility (ESRF, Grenoble). All data were collected in Debye−Scherrer geometry, using a wavelength of 0.3999 Å (31 keV). LaB_6 was applied as internal standard. The sample was sealed in a 0.5 mm quartz capillary under argon atmosphere and it was heated using a hot air blower at a constant heating rate of 5 K·min^{-1}. Diffraction data were recorded from 300 to 1123 K (2θ range 3−10°, step size 0.005°), covering the entire temperature range of stability of β-Si(NCN)$_2$.

The evolution of the lattice parameter of β-Si(NCN)$_2$ with temperature was determined by the Le Bail method, included in the program FullProf. In total, 32 refinements were performed, comprising the diffraction patterns measured from 500 to 1123 K. To obtain comparable results, the refinement at each temperature was carried out using the same procedure.

Computational. All calculations were performed in the framework of density functional theory as implemented in the Vienna Ab Initio Simulation Package (VASP). For structure optimizations we use the generalized gradient approximation (GGA) and standard pseudopotentials for Si, C, and N as supplied in the VASP package. The wave function is expanded into a plane wave basis set using an energy cutoff E_{cut} of 500 eV. Brillouin-zone integration is performed using a 4 × 4 × 4 k-point mesh. The same approach is used to calculate the vibrational modes of the crystal structure by finite difference technique. Inspection of the eigenmodes allowed us to interpret the vibrational spectra received during subsequent simulations.

Ab initio molecular dynamics (aiMD) simulations were carried out within the GGA using the standard pseudopotential for Si and soft pseudopotentials for C and N. The energy cutoff E_{cut} was set to 400 eV. The Brillouin zone was sampled at the Γ-point only. These parameters ensure that Pulay forces are negligible and do not contribute to the stress tensor. Throughout our aiMD simulations we used a time step Δt = 1 fs for the integration of the equations of motion. The temperature is controlled using a Nosé thermostat. We verified stresses and pressures to be reliable by comparison to results obtained with harder pseudopotentials, higher energy cutoff E_{cut} (500 eV), and smaller time step Δt = 0.5 fs. Calculations using the LDA provide similar results, however, with smaller lattice parameters.

We explored the thermal properties of Si(NCN)$_2$ using a 2 × 2 × 2 supercell of β-Si(NCN)$_2$ (112 atoms) in a cubic simulation box. Further details are given in the Supporting Information. We applied the same computational strategy to study the thermal expansion of cubic β-SiC. We obtain a positive linear thermal expansion coefficient α_L of 6 × 10^{-6} K^{-1} for β-SiC for the range from 300 to 900 K. This falls in with experimental values for α_L of 3.8 × 10^{-6} K^{-1} at 300 K, 4.3 × 10^{-6} K^{-1} at 600 K, and 4.8 × 10^{-6} K^{-1} at 900 K.[21,22]

dx.doi.org/10.1021/jp2106583 |J. Phys. Chem. C XXXX, XXX, 000–000

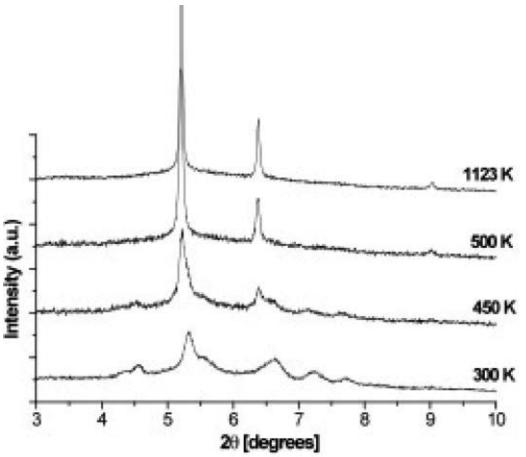

Figure 2. X-ray diffraction profiles of $Si(NCN)_2$ during heating from 300 to 1123 K in an argon atmosphere.

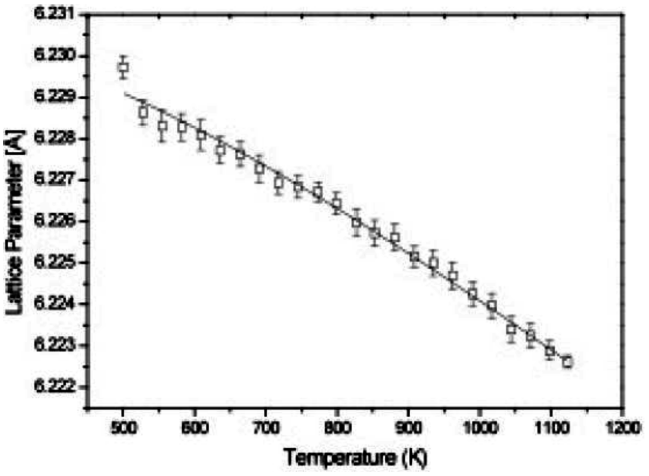

Figure 3. Evolution of the lattice parameter of β-$Si(NCN)_2$ as a function of temperature, obtained from Le Bail refinements.

RESULTS

The progressive phase transition of $Si(NCN)_2$ is represented in Figure 2 by the X-ray diffraction profiles at specific temperatures during the heating process (from 300 to 1123 K). The diffraction pattern of the room-temperature phase, α-$Si(NCN)_2$, displays broad lines. It was not possible to determine the correct symmetry for the structure by simply analyzing the diffractogram. At 450 K, changes in the profile are easily noticeable, as the transition to the high-temperature modification of $Si(NCN)_2$ starts to take place. It can be assumed that at 500 K the phase transition was completed, revealing the expected cubic structure (space group $Pn\bar{3}m$), with no secondary phases present. With increasing temperature, shifts in peak position are hardly perceptible, but there are significant changes in peak intensities, indicative of an enhanced crystallinity.

The evolution of the lattice parameter of β-$Si(NCN)_2$ as a function of temperature is shown in Figure 3. The error bars correspond to the standard deviations as obtained from the Le Bail refinement. The results indicated that β-$Si(NCN)_2$ contracts continuously upon heating from 500 to 1123 K, leading to a total decrease in the lattice parameter of 0.12%.

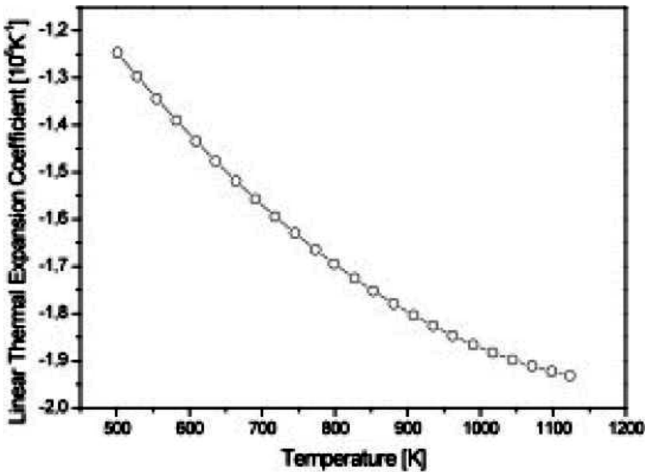

Figure 4. Linear thermal expansion coefficient of β-$Si(NCN)_2$ as a function of temperature.

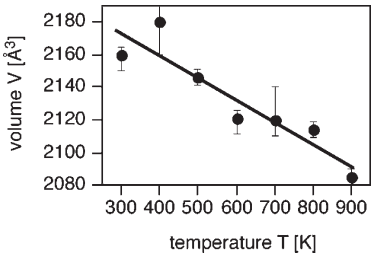

Figure 5. Zero-pressure volume of β-$Si(NCN)_2$ as a function of temperature pressure. The line is a linear fit to the data yielding the thermal expansion coefficient.

The total set of experimental data points was fitted to a third-order polynomial function: $\alpha(T) = 6.229732 - 9.68137 \times 10^{-9}\ T^2 + 2.571 \times 10^{-12}\ T^3$ [Å]. The first polynomial coefficient was set to zero as required by the boundary conditions: $\alpha \rightarrow 0$ for $T \rightarrow 0$ K. The $\alpha(T)$ curve is presented in Figure 4. Accordingly, β-$Si(NCN)_2$ displays a pronounced negative thermal expansion throughout its temperature stability range ($\alpha = -1.2468 \times 10^{-6}\ K^{-1}$ at 500 K and $\alpha = -1.9317 \times 10^{-6}\ K^{-1}$ at 1123 K).

Ab initio molecular dynamics simulation at a temperature of 300 K and a volume of 2211.5 $Å^3$ yields an isotropic negative pressure of −0.38 GPa acting on the structure of β-$Si(NCN)_2$. Increasing temperature increases the tensile stress to −1.4 GPa at 1000 K, much to our surprise. Moreover, aiMD simulations of the tetragonal structure ($P\bar{4}n2$) in a cubic simulation box yield isotropic stresses at temperatures above 300 K. In addition, averaged atomic positions become consistent with cubic symmetry in space group $Pm\bar{3}m$. We obtain Si in Wyckoff position 2a (0,0,0), C in 4b ($^1/_4,^1/_4,^1/_4$), and N in 8e (x,x,x with $x = 0.147$, at 500 K). Space group symmetry and positional parameters are matching experimental values of β-$Si(NCN)_2$, which exists between 500 and 1123 K.

Simulations at constant temperature but different volumes are then used to determine the zero pressure volume V_0 of β-$Si(NCN)_2$ for a given temperature. Data for individual results at T = 300, 500, 700, and 900 K are given in the Supporting Information. They evidence unambiguously that β-$Si(NCN)_2$ contracts at higher temperatures. A decrease of the zero-pressure volume V_0 of the supercell from 2160 to 2085 $Å^3$ upon temperature increase

dx.doi.org/10.1021/jp2106583 |J. Phys. Chem. C XXXX, XXX, 000–000

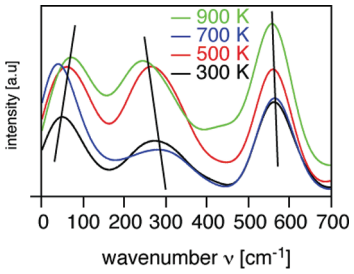

Figure 6. Low-frequency part of the vibrational spectrum of β-$Si(NCN)_2$ computed by Fourier transformation of the velocity autocorrelation function obtained at different temperatures. The height of the plots (intensity) is not normalized.

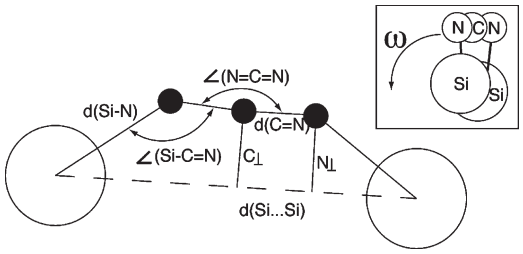

Figure 7. Geometry of the Si−NCN−Si linkage in $Si(NCN)_2$ with indication of structural parameters. The inset in the upper right corner shows a view of the group along the Si...Si direction. The angle ω characterizes the angular position of the C atom (representing the NCN group) around the Si...Si direction. Details on ω are given in the Supporting Information.

from 300 to 900 K, respectively, corresponds to a volume expansion coefficient a_V of approximately -6×10^{-5} K^{-1}. Collecting our results of V_0 from simulations at temperatures between 300 and 900 K in Figure 5, we can perform a linear fit to the data. It yields $V = 2214.4 \times (1 - 62 \times 10^{-6} \times T/K)$ Å^3, with T the temperature during simulation. For the linear expansion coefficient α we obtain $-20 \times 10^{-6} \pm 3 \times 10^{-6}$ K^{-1}, with the error resulting from the least-squares fit.

Therefore, while static density functional calculations in both LDA and GGA yield a tetragonal ground-state structure for $Si(NCN)_2$ [18], dynamic simulation of $Si(NCN)_2$ at elevated temperatures indicate an isotropic cubic crystal. The time-averaged crystallographic data is in full agreement with experimental results. The NTE effect observed in simulations also resolves the puzzle of the large overestimation of lattice parameter in static calculations. We find a lattice parameter of cubic β-$Si(NCN)_2$ of 6.45 Å at 500 K, which is only 4% larger than the experiment. Such minor discrepancy can be expected for the GGA functional used.

To analyze the foundation for the observed negative thermal expansion, we first investigate the vibrational spectrum of β-$Si(NCN)_2$. We obtained this from dynamical simulations at various temperatures through the velocity autocorrelation function. The low-frequency part of the spectrum, shown in Figure 6, is characterized by three major branches: one centered around 70 cm^{-1}, a second between 200 and 350 cm^{-1}, and a third branch at about 560 cm^{-1}. The latter is due to symmetrical bond bending of the N═C═N unit, sometimes also referred to as Si−N═C═N vibrations.[19] The position of the maximum of this branch is not affected by temperature. In contrast, vibrations in the region between 200 and 350 cm^{-1} depend strongly on temperature. As temperature increases, the maximum of this branch shifts toward lower wave numbers. Modes in this region are related to vibrations of rigid N═C═N moieties between Si atoms bonded to it. Eigenvector calculations (of the tetragonal zero-temperature structure) confirm this assignment. Modes between 0 and 100 cm^{-1} are related to concerted rotations (tumbling) of SiN_4 tetrahedra. This branch appears to be only slightly affected by temperature.

Therefore, we find that modes of the branch between 200 and 350 cm^{-1} decrease in frequency when temperature is increased. They constitute rigid unit modes (RUMs) with negative mode-Grüneisen parameters. In the context of NTE effects, they contribute to an overall negative thermal expansion coefficient.

Eigenvector calculations together with simulation data let us infer that transverse NCN motions, in the form of librations, go along with translations of the low-energy modes and appear almost inseparable. Both the rotations of SiN_4 tetrahedra and the vibrations of rigid N═C═N moieties appear at low wave numbers because the Si−N═C bond angle potential is very shallow and soft. A mixing thus arises due to the low constrained NCN unit and the openness of the structure. The mixing may be crucial to the mechanism of the NTE: the transverse NCN motion provides the thermal motion that contracts the lattice; the presence of a translational component in each low-energy mode provides a source of frustration that inhibits lattice instabilities that would destroy NTE.

Table 1. Structural Parameters Obtained from Simulations at Different Temperatures[a]

parameter	300 K	500 K	700 K	900 K
d(Si−N)	169.5	170.0	170.5	171.0
d(N═C)	121.1	121.2	121.4	121.7
∠(N═C═N)	173.5	171.8	170.8	169.4
∠(Si−N═C)	157.0	155.3	153.3	150.9
∠(Si...C...Si)	166.7	166.1	165.1	163.7
d(Si...Si)	562.8	561.6	559.6	556.2
$N_\perp$	41.3	43.4	46.4	50.3
$N_\parallel$	163.2	163.0	162.5	161.5
$C_\perp$	32.6	34.1	36.4	39.7

[a] Distances are given in pm and angles in degrees (°).

To extend our understanding for the contraction of the structure upon heating, we further develop detailed insight of the atomistic structure of β-$Si(NCN)_2$. We first re-emphasize the significant difference between instantaneous and averaged structure. The instantaneous structure, a snapshot taken at a point during simulation, does not exhibit cubic symmetry or linear angles. These high-symmetry features are established after first averaging the atomic positions in the crystal over time and only then computing structural parameters. In particular, we focus on some important internal parameters along the linkage between two Si atoms in the β-$Si(NCN)_2$ structure, as indicated in Figure 7. This local reference frame, extricated from vibrational motions of both Si atoms, is very helpful to develop a simple mechanistic picture of the NTE effect.

If structural parameters in the local reference frame are calculated every time step and only then averaged over time (and sites in the structure), we obtain the data given in Table 1.

According to Table 1, Si−N and C═N bond distances increase with increasing temperature. This is expected by a typical anharmonic bonding potential. On the other hand, the distance

dx.doi.org/10.1021/jp2106583 |J. Phys. Chem. C XXXX, XXX, 000–000

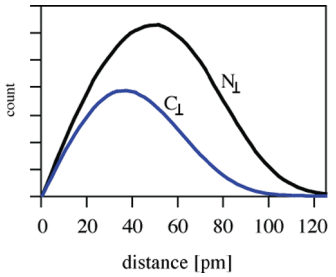

Figure 8. Probability distributions of $C_\perp$ and $N_\perp$ (at 900 K) characterizing the distance of C and N from the Si...Si connection line, respectively (see Figure 7). Maxima are located at 36 and 49 pm for C and N, respectively.

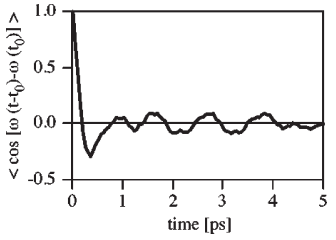

Figure 9. Autocorrelation function for the angle ω characterizing the time development of the orientation of the NCN unit around the Si...Si connection line (at 900 K).

between two Si atoms bridged by a NCN unit (Si−NCN−Si), about 560 pm, decreases with increasing temperature. A reduction of this parameter by 6.6 pm between 300 and 900 K reflects the negative linear thermal expansion. This decrease of the Si...Si distance goes together with a decrease of the Si−N═C bond angle. Two additional parameters, $N_\perp$ and $C_\perp$ are included in Table 1. They characterize the distance of N and C from the Si...Si connection line, respectively. Figure 8 shows a probability distribution of $C_\perp$ and $N_\perp$ at 900 K. Apparently, neither C nor N are located at the line between the two Si at any given time. Since both parameters increase with increasing temperature, the complete NCN group moves off the Si...Si connection with increasing temperature. This mechanism matches that of proposed transverse displacements of cyanide bridges in $Zn(CN)_2$.[23]

While the NCN unit is located off the Si...Si connection line and vibrating transverse to it, it also rotates around the Si...Si connection line. This movement is characterized by an angle ω (defined in the inset to Figure 7 and more clearly in the Supporting Information). Of course, rotation of *one* NCN group will cause a concerted movement of *all* NCN groups because of tetrahedral bond angles at SiN_4 units, which provide some constraint.

Figure 9 then displays the angular autocorrelation function of ω. The fast decrease from 1 (strongly correlated orientation) indicates that the NCN unit tumbles freely around the reference connection between the two Si atoms. The residual oscillation indicates a concerted rotation of all NCN units around their respective references approximately every 1 ps, corresponding to a wave number of 33 cm^{-1}. This fits very well into the low-frequency region seen in Figure 6. The rotation is not monotonous, however. Instead, the rotation direction of an individual NCN unit may change from clockwise to counterclockwise, as seen when ω for an individual NCN unit is plotted versus time (see Supporting Information). Coalescing this information, we conclude that the NCN group rotates around the reference frame provided by the two Si atoms, between which the NCN unit bonds. The rotation is not consistent, but frequently reverses its direction. Nevertheless, the angular phase space is visited evenly. Since there is vanishing probability to locate an atom at the central axis (see Figure 8), the distribution of the probability to find an atom of the NCN group in the reference frame forms a torus/doughnut. The inner diameter of this torus increases with increasing temperature.

DISCUSSION

β-$Si(NCN)_2$ displays negative thermal expansion throughout its temperature stability range, the linear expansion coefficient increasing in magnitude from $\alpha = -1.24 \times 10^{-6}\ K^{-1}$ at 500 K to $\alpha = -1.93 \times 10^{-6}\ K^{-1}$ at 1123 K. Like β-$Si(NCN)_2$, NTE has been observed for materials that share the relatively simple cuprite structure, including the oxides Cu_2O and Ag_2O.[24,25] Other nonoxide materials, $Zn(CN)_2$ and $Cs(CN)_2$, which are structurally similar to β-$Si(NCN)_2$, also show similar thermal expansion, albeit in a smaller temperature regime and at lower temperatures up to 375 K only.[11,12] Whereas the cyanide unit (CN) plays a crucial role in the NTE behavior of $Zn(CN)_2$, the carbodiimide moiety (—N═C═N—) accounts for it in β-$Si(NCN)_2$.

Ab initio molecular dynamics predict $\alpha = -20 \times 10^{-6} \pm 3 \times 10^{-6}\ K^{-1}$ for the ideal infinite crystal. Though a difference of an order of magnitude to experimental results may appear large at first, cooling data obtained for the same material (given in the Supporting Information) show only a discrepancy of a factor of 3. It is unclear whether a disagreement is due more to the ab initio simulations or to experiment. Experimentally, small nanocrystals were studied, with imperfections and surface effects probably reducing the NTE behavior. It is worthy to note that compared to previous studies,[20] we were successful in improving the quality of the compound, and that the improvement went along with a higher NTE effect. This may be an indication that the simulation catches correctly the effect for the ideal crystal, while actual sample conditions tend to reduce the NTE effect.

The NTE originates from vibrations of rigid N═C═N moieties between Si atoms. These vibrations are both rotational and transverse in nature. Concerted NCN motions pull Si atoms, between which the NCN bonds, closer together. Upon temperature increase, the bridging NCN units move outward from the direct connection between the Si atoms, thus reducing the Si...Si distance. This detailed atomistic analysis of the NTE effect allows us to locate the origin of NTE in β-$Si(NCN)_2$ and to develop a simplified mechanical picture: we observe a centrifugal governor at the atomistic level.

SUMMARY

In summary, a systematic investigation on the thermal behavior of β-$Si(NCN)_2$ has been carried out in the present work. Dynamical simulations and high-temperature synchrotron crystallography show that β-$Si(NCN)_2$ exhibits negative thermal expansion from 500 to 1123 K. The NTE effect originated from transverse vibrations of carbodiimide fragments bridging between Si atoms (Si−N═C═N−Si). The concerted movements of atoms have much in common with an ensemble of atomistic centrifugal governors that pull together the crystal framework upon temperature increase. The present study may motivate additional interest in carbodiimide chemistry to develop compounds with NTE at even lower temperatures than the title compound.

dx.doi.org/10.1021/jp2106583 |*J. Phys. Chem. C* XXXX, XXX, 000–000

■ ASSOCIATED CONTENT

Supporting Information. Diffraction data from heating and cooling runs, details of the computational procedure, images and analyses of selected vibrational modes, and definition of rotovibrational parameters. This material is available free of charge via the Internet at http://pubs.acs.org.

■ AUTHOR INFORMATION

Corresponding Author
*pkroll@uta.edu.

■ ACKNOWLEDGMENT

We thank ESRF for providing radiation beam time on the beamline ID31. The work has been financially supported by the German Science Foundation under the Priority Program SPP 1236 "Strukturen und Eigenschaften von Kristallen bei extrem hohen Drücken und Temperaturen". R.R. thanks the Fonds der Chemischen Industrie for continuous support. The computational work was made possible through generous grants by the Texas Advanced Computing Center in Austin, TACC, Texas, and by the High Performance Computing Center at UTA. P.K. is supported by the NSF (DMR-0907117) and by the U.S. AFOSR and NASA under the National Hypersonics Science Center for Materials and Structures (AFOSR Contract No. FA9550-09-1-0477).

■ REFERENCES

(1) Fornasini, P.; Dalba, G.; Grisenti, R.; Purans, J.; Vaccari, M.; Rocca, F.; Sanson, A. *Nucl. Instrum. Meth. B* **2006**, *246*, 180.
(2) Barrera, G. D.; Bruno, J. A. O.; Barron, T. H. K.; Allan, N. L. *J. Phys.-Condens. Matter* **2005**, *17*, R217.
(3) Evans, J. S. O. *J. Chem. Soc. Dalton* **1999**, 3317.
(4) Hao, Y. M.; Gao, Y.; Wang, B. W.; Qu, J. P.; Li, Y. X.; Hu, J. F.; Deng, J. C. *Appl. Phys. Lett.* **2001**, *78*, 3277.
(5) Evans, J. S. O.; David, W. I. F.; Sleight, A. W. *Acta Crystallogr. B* **1999**, *55*, 333.
(6) Salvador, J. R.; Gu, F.; Hogan, T.; Kanatzidis, M. G. *Nature* **2003**, *425*, 702.
(7) Miller, W.; Smith, C. W.; Mackenzie, D. S.; Evans, K. E. *J. Mater. Sci.* **2009**, *44*, 5441.
(8) Sleight, A. W. *Annu. Rev. Mater. Sci.* **1998**, *28*, 29.
(9) Evans, J. S. O.; Mary, T. A.; Vogt, T.; Subramanian, M. A.; Sleight, A. W. *Chem. Mater.* **1996**, *8*, 2809.
(10) Mary, T. A.; Evans, J. S. O.; Vogt, T.; Sleight, A. W. *Science* **1996**, *272*, 90.
(11) Williams, D. J.; Partin, D. E.; Lincoln, F. J.; Kouvetakis, J.; O'Keeffe, M. *J. Solid State Chem.* **1997**, *134*, 164.
(12) Goodwin, A. L.; Kepert, C. J. *Phys. Rev. B* **2005**, *71*, 140301.
(13) Pryde, A. K. A.; Hammonds, K. D.; Dove, M. T.; Heine, V.; Gale, J. D.; Warren, M. C. *J. Phys.-Condens. Matter* **1996**, *8*, 10973.
(14) Evans, J. S. O.; Hu, Z.; Jorgensen, J. D.; Argyriou, D. N.; Short, S.; Sleight, A. W. *Science* **1997**, *275*, 61.
(15) Evans, J. S. O.; Hanson, P. A.; Ibberson, R. M.; Duan, N.; Kameswari, U.; Sleight, A. W. *J. Am. Chem. Soc.* **2000**, *122*, 8694.
(16) Kessler, V. G.; Panov, A. N.; Borissevitch, A. Y.; Turova, N. Y. *J. Sol-Gel Sci. Techn.* **1998**, *12*, 81.
(17) Riedel, R.; Greiner, A.; Miehe, G.; Dressier, W.; Fuess, H.; Bill, J.; Aldinger, F. *Angew. Chem.-Int. Ed. Engl.* **1997**, *36*, 603.
(18) Kroll, P.; Riedel, R.; Hoffmann, R. *Phys. Rev. B* **1999**, *60*, 3126.
(19) Riedel, R.; Kroke, E.; Greiner, A.; Gabriel, A. O.; Ruwisch, L.; Nicolich, J.; Kroll, P. *Chem. Mater.* **1998**, *10*, 2964.
(20) Riedel, R.; Horvath-Bordon, E.; Kleebe, H. J.; Kroll, P.; Miehe, G.; van Aken, P. A.; Lauterbach, S. *J. Chin. Ceram. Soc.* **2007**, *35*, 955.
(21) Goldberg, Yu.; Levinshtein, M.; Rumyantsev, S. In *Properties of Advanced Semiconductor Materials GaN, AlN, SiC, BN, SiC, SiGe*; Levinshtein, M. E., Rumyantsev, S. L., Shur, M. S., Eds.; John Wiley & Sons, Inc.: New York, 2001; p 93.
(22) Kern, E. L.; Hamill, D. W.; Deem, H. W.; Sheets, H. D. *Mater. Res. Bull.* **1969**, *4*, S25.
(23) Chapman, K. W.; Chupas, P. J.; Kepert, C. J. *J. Am. Chem. Soc.* **2005**, *127*, 15630.
(24) Tiano, W.; Dapiaggi, M.; Artioli, G. *J. Appl. Crystallogr.* **2003**, *36*, 1461.
(25) Sanson, A.; Rocca, F.; Dalba, G.; Fornasini, P.; Grisenti, R.; Dapiaggi, M.; Artioli, G. *Phys. Rev. B* **2006**, *73*, 13.